

A Diffeomorphic Approach to Multimodal Registration with Mutual Information: Applications to CLARITY Mouse Brain Images

Kwame S. Kutten¹, Nicolas Charon¹, Michael I. Miller¹, J. Tilak Ratnanather¹, Karl Deisseroth², Li Ye², and Joshua T. Vogelstein¹

¹Johns Hopkins University, Baltimore, MD, USA

²Stanford University, Stanford, CA, USA

{kwame, charon, mim, tilak, jovo}@cis.jhu.edu, {deissero, liye02}@stanford.edu

Abstract

Large Deformation Diffeomorphic Metric Mapping (LDDMM) is a widely used deformable registration algorithm for computing smooth invertible maps between various types of anatomical shapes such as landmarks, curves, surfaces or images. In this work, we specifically focus on the case of images and adopt an optimal control point of view so as to extend the original LDDMM with Sum of Squared Differences (SSD) matching term to a framework more robust to intensity variations, which is critical for cross-modality registration. We implement a mutual information based LDDMM (MI-LDDMM) algorithm and demonstrate its superiority to SSD-LDDMM in aligning 2D phantoms with differing intensity profiles. This algorithm is then used to register CLARITY mouse brain images to a standard mouse atlas despite their differences in grayscale values. We complement the approach by showing how a cascaded multi-scale method improves the optimization while reducing the run time of the algorithm.

1. Introduction

1.1. Deformable Image Registration

The problem of deformable registration is as follows. Let $\Omega \subset \mathbb{R}^3$ be the background space. Given template image $I_0 : \Omega \rightarrow \mathbb{R}$ and target image $J_1 : \Omega \rightarrow \mathbb{R}$ we seek a non-linear map φ such that $I_0 \circ \varphi^{-1}$ is aligned to J_1 . In medical and biological imaging, deformations need to account for a large variety of local morphological variations and φ should ideally be modeled as a *diffeomorphism*, i.e a differentiable coordinate transform with differentiable inverse, in which case φ represents a one-to-one correspondence between anatomy in I_0 and anatomy in J_1 . Many different

models have been proposed in the past to generate and estimate diffeomorphic transformations including the B-splines framework of [30], polyaffine transformations as in [3] or diffeomorphic demons [34].

1.2. LDDMM

The Large Deformation Diffeomorphic Metric Mapping (LDDMM) is another of these models that has been widely used due to its versatility. Introduced by Beg *et al.* for registration of dense images [7], it has been generalized to a wide array of geometric objects including landmarks [22], unlabeled point distributions [17], curves and surfaces [33, 12], diffusion tensor [10] and multi-channel images [11].

In image registration, Beg *et al.* uses a time varying velocity field $v : [0, 1] \times \Omega \rightarrow \mathbb{R}^3$ to flow I_0 at time 0 to the coordinate system of J_1 at time 1. Diffeomorphic map $\phi_{ts} : \Omega \rightarrow \Omega$ represents the coordinate transform from time $t \in [0, 1]$ to time $s \in [0, 1]$. It is defined using the following differential equation

$$\frac{d}{dt}\phi_{st} = v(t, \phi_{st}) \quad (1)$$

in which through integration we see that

$$\phi_{st} = id + \int_s^t v(\tau, \phi_{s\tau}) d\tau \quad (2)$$

where $id : \Omega \rightarrow \Omega$ defined as $id(x) = x$ is known as the identity mapping [7].

Let $I(t) = I_0 \circ \phi_{t0}$ be the deformed template at time t . LDDMM minimizes the functional

$$E(v) = R(v) + \frac{1}{2\sigma^2} M(I(1), J_1) \quad (3)$$

where $M(I(1), J_1)$ is a matching term that is minimized when deformed template $I(1)$ is aligned with target J_1 .

In Beg *et al.* the matching term is defined as the Sum of Squared Differences (SSD) between $I(1)$ and J_1 .

$$\begin{aligned} M(I(1), J_1) &= \|I(1) - J_1\|_{L^2}^2 \\ &= \int_{\Omega} (I(1, x) - J_1(x))^2 dx \end{aligned} \quad (4)$$

Regularization term $R(v) = \frac{1}{2} \int_0^1 \|Lv(t)\|_{L^2}^2 dt$ with differential operator $L = \alpha \nabla^2 + id$ ensures that v and thus its corresponding map is smooth. Constant $\alpha \in \mathbb{R}$ determines the smoothness of the transform while $\sigma \in \mathbb{R}$ determines the weight of the matching term M relative to regularization term R . Typically, the choice of this parameter depends on the level of noise in the images as well as the smoothness of the mappings that are sought [7].

Beg *et al.* minimized functional (3) using a variational approach. Euler-Lagrange equations for the functional were written and an expression for gradient $\nabla_v E$ was derived. Thus optimal v was estimated using the gradient descent scheme $v = v - \varepsilon \nabla_v E$ where ε controls the step size [7]. The alternative approach of [35] proposes instead a formulation based on Hamiltonian systems and a geodesic shooting procedure on the initial momentum to solve the LDDMM-SSD problem.

1.3. Mutual Information

A major drawback to SSD image matching is that it can only be used to align images with similar intensity profiles. Since it is based on image subtraction it assumes that bright regions should be aligned to bright regions while dark regions should be matched to dark regions. While this assumption is sufficient for images of the same modality (*e.g.* aligning MR to MR images) it fails in registering images of different intensity profiles (*e.g.* MR to CT images). This assumption is also routinely violated in the microscopy world in which a wide variety of stains and fluorescent labels are used to generate images that vary greatly in appearance. Thus one way this problem has been addressed in MR-CT diffeomorphic registration is through modality independent neighborhood descriptors [28, 29].

In this work we propose replacing SSD matching with Mutual Information (MI) for alignment of images generated by light-sheet microscopy to standard atlases. Roughly speaking the MI between a pair of random variables is the reduction of uncertainty in the first random variable when given the second one [14, 27]. In image registration the pair of random variables represent the intensities of the template and target images. The goal is to find map φ which results in the greatest reduction of uncertainty in template $I_0 \circ \varphi^{-1}$ when given target J_1 . Since MI depends on uncertainty, reduction and not explicitly on the grayscale values, it can be used to align corresponding image regions regardless of whether they share intensity values.

For image matching with LDDMM we define the matching term as the negative MI

$$\begin{aligned} M(I(1), J_1) &= - \int_{-\infty}^{\infty} \int_{-\infty}^{\infty} p_{IJ}(\eta, \xi) \cdot \\ &\quad \log \left(\frac{p_{IJ}(\eta, \xi)}{p_I(\eta)p_J(\xi)} \right) d\eta d\xi \end{aligned} \quad (5)$$

where $\eta \in \mathbb{R}$ and $\xi \in \mathbb{R}$ are intensity values from $I(1)$ and J_1 respectively. Distributions $p_I(\eta)$, $p_J(\xi)$ and $p_{IJ}(\eta, \xi)$ are the deformed template, target and joint histograms of the images. The subscripts I and J denote dependence on $I(1)$ and J_1 respectively.

Mutual Information (MI) has found many applications in affine [36] and diffeomorphic image registration [27]. In the context of large deformation diffeomorphic registration, Avants *et al.* developed the open source Advanced Normalization Tools (ANTs). ANTs implements a symmetric version of Beg *et al.* that supports SSD, MI and Cross Correlation matching terms but in which the matching term is evaluated in the middle of the time domain (at $t = 0.5$) instead of at its end point (at $t = 1$) [4, 5]. Code for these matching terms were contributed the open source Insight Segmentation and Registration Toolkit (ITK) [6, 20].

In this work, as we explain in the following section, our interest is rather in the registration of subjects to a template of a different modality, in which case the symmetry of the mapping is not necessarily a relevant property. Thus, the approach of this paper is rather to propose an extension of the standard LDDMM pipeline for multi-modality.

1.4. CLARITY

CLARITY is a novel technique which converts biological tissues into translucent and porous hydrogel-tissue hybrids. This permits the penetration of photons and molecular probes. The procedure works by eliminating lipid barriers which block fluorescent antibodies and scatter light. Thus CLARIFIED tissues can then be immunostained and imaged using light sheet microscopy without mechanical slicing [13, 23, 32].

To extract meaningful spatial information from these images (*e.g.* number of fluorescent cell bodies in L. Hippocampus), they need to be registered to a standard atlas. An atlas usually consists of an atlas image and corresponding annotations for anatomical structures. Although many mouse brain atlases have been developed, including those based on Magnetic Resonance [19], Computed Tomography [15] and Nissl-stained [16] images, to our knowledge no CLARITY atlas exists due to the novelty of the technique. This matter is further complicated by the fact that the appearance of CLARITY volumes may vary greatly due to the choice of antigens, fluorescent antibodies and imaging parameters. Thus Nissl-stained atlas to CLARITY reg-

istration using SSD matching has been shown to give poor results [24].

A proposed workaround to this problem was to register the segmented mask volume of the CLARITY image to the segmented mask volume of the atlas image. Only edge information is used and gray level values within the template and target brains are ignored. While this method could accurately align the superficial cortical structures its practical application was limited due to misalignment of deeper brain structures [24].

In contrast, we present here the very first results of registration between CLARITY brains onto the Allen Reference Atlas (ARA) using MI-LDDMM. The ARA was created as the reference space of gene expression data for the adult mouse Allen Brain Atlas [1, 21]. The current version of the ARA was constructed by averaging the shape and intensity of over 1600 mouse brain specimens acquired through Serial Two Photon Tomography [2].

1.5. Contributions

The main contributions of this work are the following. In sections 2.1-2.2 we rederive the dynamics of LDDMM from an optimal control perspective and show how it can be generalized conveniently to matching terms other than SSD. We then implement an extension of the original LDDMM image registration algorithm in 2.5 that include both MI and SSD image registration. In section 3.2 we compare both approaches for registering mouse brains imaged using CLARITY-Optimized Light-sheet Microscopy (COLM) to a standard atlas. Finally, in section 3.3, we evaluate a possible improvement of the algorithm run time and global convergence properties that relies on a cascaded multi-scale approach.

2. Methods

2.1. Optimal Control Problem

With the notations of the introduction, we can interpret registration in the LDDMM setting as an optimal control problem where the state is the template image evolution $I(t) = I_0 \circ \phi_{t0}$ and the control is the velocity field $v(t, \cdot)$. This evolution is equivalently described by an advection equation. Indeed, differentiating with respect to t and using (1), we have:

$$\begin{aligned} \partial_t I(t, \cdot) &= (\nabla I_0) \circ \phi_{t0} \cdot \partial_t \phi_{t0} \\ &= (\nabla I_0) \circ \phi_{t0} \cdot (-d\phi_{0t} \circ \phi_{t0})^{-1} v(t, \cdot) \\ &= -\nabla(I_0 \circ \phi_{t0}) \cdot v(t, \cdot) \\ &= -\nabla I(t) \cdot v(t) \end{aligned}$$

Thus we can write the LDDMM problem as:

$$v^* = \arg \min_v \{E(v) : \partial_t I = -\nabla I \cdot v, I(0) = I_0\} \quad (6)$$

The corresponding Hamiltonian is obtained classically by introducing the costate function ρ in L^2 associated to the constraints, leading to:

$$H(\rho, I, v) = -\langle \rho, \nabla I \cdot v \rangle_{L^2} - \frac{1}{2} \|Lv\|_{L^2}^2 \quad (7)$$

2.2. Optimal Control Solution

Following Miller *et al.*, with Pontryagin's Maximum Principle [26], we know that the dynamics of optimal solutions to (6) are governed by the following system of coupled Hamiltonian equations:

$$\partial_t I = \partial_\rho H \quad (8a)$$

$$\partial_t \rho = \partial_I H, \quad \rho(1) = -\frac{1}{2\sigma^2} \partial_I M(I(1), J_1) \quad (8b)$$

$$\partial_v H = 0 \quad (8c)$$

From this, we obtain the following set of equations for our problem:

$$I(t) = I_0 \circ \phi_{t0} \quad (9a)$$

$$\rho(t) = -\frac{1}{2\sigma^2} \left(\partial_I M(I(1), J_1) \circ \phi_{t1} \right) |D\phi_{t1}| \quad (9b)$$

$$0 = v + K(\rho \nabla I) \quad (9c)$$

where we have defined

$$K = (L^\dagger L)^{-1}. \quad (10)$$

Equation (9a) is immediately obtained from (8a) using the advection equation in (6). We derive (9b) from (8b) by evaluating $\partial_I H$

$$\begin{aligned} (\partial_I H | \delta I) &= -(\partial_I \nabla I \cdot (\rho v) | \delta I) \\ &= -(\partial_I (\nabla \cdot (I \rho v) - I \nabla \cdot (\rho v)) | \delta I) \end{aligned}$$

Where we have taken advantage of the identity $\nabla \cdot (fF) = f \nabla \cdot F + \nabla f \cdot F$ for $f : \mathbb{R}^d \rightarrow \mathbb{R}$ and $F : \mathbb{R}^d \rightarrow \mathbb{R}^d$. Using the divergence theorem and assuming that v vanishes along the boundary of the background space $\partial\Omega$ we see that

$$\begin{aligned} (\partial_I H | \delta I) &= (\partial_I I \nabla \cdot (\rho v) | \delta I) \\ &= (\nabla \cdot (\rho v) | \delta I) \end{aligned}$$

Applying equation (8b) gives us the differential equation

$$\partial_t \rho = \nabla \cdot (\rho v) \quad (11)$$

from which by we can show that

$$\rho(t, x) = \rho(1, \varphi_{t1}) |D\varphi_{t1}|$$

is a solution to differential equation (11) [18, 26] that satisfy the same endpoint condition at $t = 1$, thus leading to Equation (9b).

Finally, we derive (9c) using (8c). By rearranging the Hamiltonian (7) we see that

$$\begin{aligned} (\partial_v H | \delta v) &= - \left(\partial_v \left(\rho \nabla I \cdot v + \frac{1}{2} L^\dagger L v \cdot v \right) \right) | \delta v \\ &= - (\rho \nabla I + L^\dagger L v | \delta v) \end{aligned}$$

which by (8b) implies

$$0 = \rho \nabla I + L^\dagger L v.$$

Equation (9c) follows using definition (10).

2.3. SSD Matching

The advantage of formulation (9) is that it lets us generalize LDDMM to any matching term as long as we can find the derivative $\partial_I M(I(1), J_1)$. For the SSD matching term, defined in (4), we find the Gâteaux derivative

$$\partial_I M(I(1), J_1) = 2(I(1) - J_1).$$

2.4. MI Matching

Using a similar procedure we can show that for MI matching term, defined in (5), we have the following gradient

$$\partial_I M(I, J_1) = - \int_{-\infty}^{\infty} \int_{-\infty}^{\infty} \partial_I p_{IJ}(\eta, \xi) \log p_{J|I}(\xi | \eta) d\eta d\xi.$$

In order to evaluate the above expression we need to estimate distributions $p_I(\eta)$, $p_J(\xi)$ and $p_{IJ}(\eta, \xi)$ in terms of $I(1)$ and J_1 . Furthermore we need to differentiate $\partial_I p_{IJ}(\eta, \xi)$. This can be done by estimating these distributions using the Mattes *et al.* method [25]. In brief $p_{IJ}(\eta, \xi)$ is approximated by using Parzen windowing. Since we need differentiability with respect to $I(1)$, 3rd order B-splines are used to estimate distributions in terms of template intensity η . On the other hand, only a 0th order B-splines are used for target intensities ξ . Distributions $p_I(\eta)$ and $p_J(\xi)$ are then found by marginalizing $p_{IJ}(\eta, \xi)$ [25].

2.5. Algorithm

Equations (9) were used to implement an LDDMM algorithm in ITK with a generalized matching term (Fig 1). We essentially iterate updates of the state, costate and control at all times t until reaching the optimality conditions of the previous section. The update on v is obtained by following the gradient $\nabla_v E = v + K(\rho \nabla I)$ (cf [7]) which leads to convergence to the condition of Equation (9c).

More specifically, the algorithm uses a discretization of the time domain $[0, 1]$ into T evenly spaced time samples such that $0 = t_0, \dots, t_{T-1} = 1$. At the beginning of each iteration, the map $\phi_{t_j, 1}$, costate $\rho(t_j)$, state $I(t_j)$ and energy

```

N = ITERATIONS, T = TIMESTEPS
ε = SMALL, v = 0
I(t_j) = I_0 ∀ j ∈ {0, T - 1}

foreach n ∈ {0, ..., N - 1}
  foreach j ∈ {T - 2, ..., 0}
    φ_{t_j, 1} = φ_{t_{j+1}, 1}(id + d_{t_{j+1}, t_j}(v))
    I(t_j) = I(1) ∘ φ_{t_j, 1}
    ρ(t_j) = -1/(2σ²) (∂_I M(I(1), J_1) ∘ φ_{t_j, 1}) | Dφ_{t_j, 1} |
    ∇_v E(t_j) = v(t_j) + K(ρ(t_j) ∇ I(t_j))

(v_{old}, E_{old}) = (v, E(v))
while (ε > ε_{min})
  v = v - ε ∇_v E
  foreach j ∈ {1, ..., T - 1}
    φ_{t_j, 0} = φ_{t_{j-1}, 0}(id - d_{t_{j-1}, t_j}(v))
  I(1) = I_0 ∘ φ_{1, 0}
  if (E(v) > E_{old})
    ε = 0.5 * ε
    v = v_{old}
  else
    ε = 1.1 * ε
    break

v* = v

```

Figure 1: LDDMM algorithm with generalized matching term. Displacement fields of the form $d_{st}(v)$ are found by integrating time varying velocity field v using semi-Lagrangian advection. Energy $E(v)$ is calculated using time discretized version of equation (3).

gradient $\nabla_v E(t_j)$ are calculated for each time step by flowing backward from time $t_{T-1} = 1$ to $t_0 = 0$. Displacement fields of the form $d_{st}(v)$ are found by integrating v from time s to t using semi-Lagrangian advection [7, 31]. This is then added to id to obtain the map.

Matching term gradient $\partial_I M(I(1), J_1)$ is computed using ITK's implementations of the SSD or MI matching terms [20]. After calculation of $\nabla_v E$, velocity v is updated using a gradient descent scheme with step size ε . Since the goal is to minimize $E(v)$, the updated v is rejected if $E(v)$ increases. The step size ε is then halved and the update is attempted again. If $E(v)$ decreased, ε is increased slightly and the algorithm advances to the next iteration. The process continues until the number of iterations N was surpassed or ε falls below the minimum acceptable value ε_{min} .

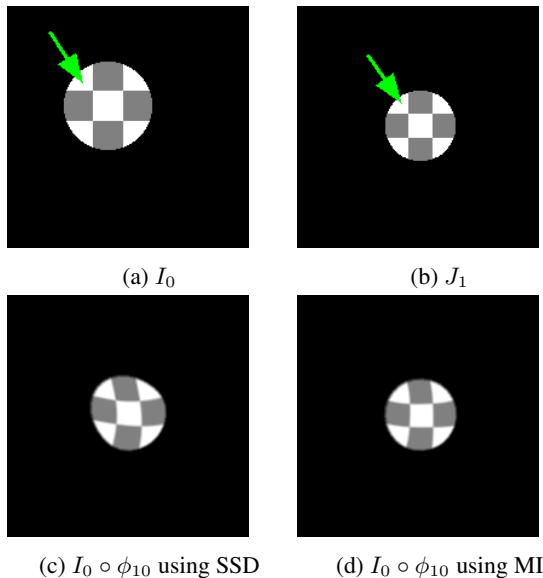


Figure 2: Experiment in which template (a) is registered to target with same intensity profile (b). This means that bright regions should be aligned to bright regions as indicated by the green arrows (a-b).

3. Experiments

3.1. 2D Phantoms

Two experiments were performed to compare the new MI-LDDMM to the original SSD-LDDMM with $\alpha = 0.02$. In the first experiment a template was matched to a target image with the same intensity profile (Fig. 2). This means that bright regions of I_0 should be matched to bright regions in J_1 . Thus the experiment simulates intramodality registration. Both algorithms gave comparable results which suggests that either could be used in intramodality registration.

In the second experiment the phantom template was matched to a target phantom with a differing intensity profile (Fig. 3). Thus bright regions in I_0 need to be aligned with dark regions of J_1 . This experiment simulates multimodality registration of images with very different gray level values. While, MI matching (Fig. 3d) gave similar results to the previous experiment (Fig. 2d), SSD registration clearly failed (3c).

3.2. 3D CLARITY images

For this work, N=11 mouse brains were CLARified and imaged using COLM following Tomer *et al.* [32]. Acquired image data for each brain was stitched using TeraStitcher [8]. At their full resolution of $0.6 \mu m \times 0.6 \mu m \times 6 \mu m$, each volume was over a terabyte in size. Since they were far to large to be analyzed on a personal computer, volumes were ingested into the NeuroData cluster, a computational

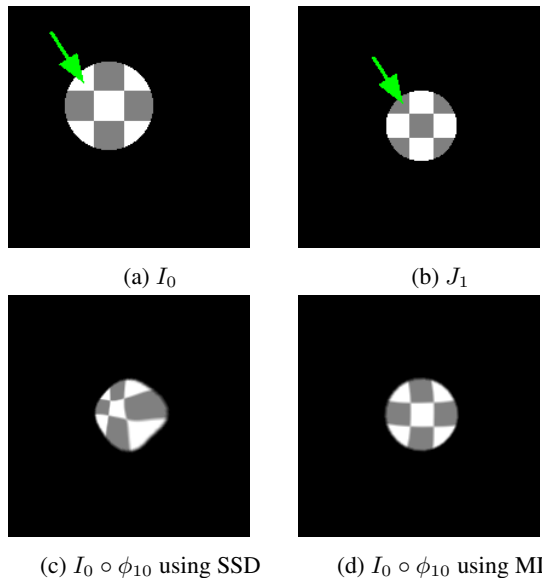


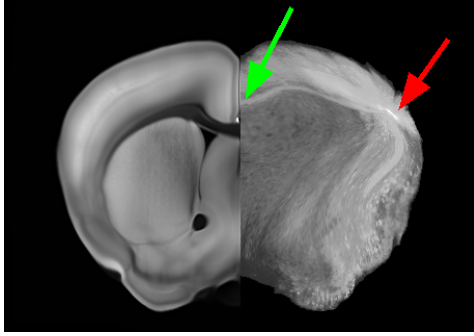
Figure 3: Experiment in which template (a) is registered to a target with a different intensity profile (b). Thus bright regions in the template should be aligned to dark regions in the target as indicated by the green arrows (a-b). Although MI matching (d) gave similar results to the previous experiment (Fig. 2d), SSD matching failed (c).

infrastructure developed for storage and retrieval of terabyte scale images [9]

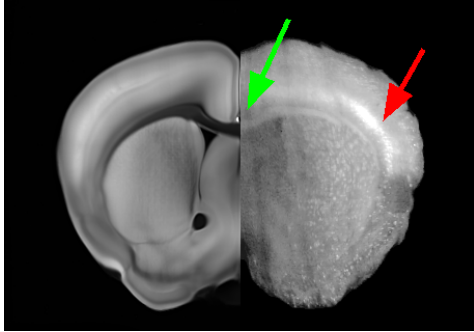
Each CLARITY volume was downloaded from the NeuroData cluster and resampled to a $50 \mu m$ resolution. After 12-parameter affine alignment, deformable registration was done using MI-LDDMM and SSD-LDDMM. A cascaded-alpha approach was adopted in which a smoother registration with $\alpha = 0.05$ was followed registrations at $\alpha = 0.02$ and $\alpha = 0.01$ to refine the results. Figure 4 compares the SSD and MI matching for one of the CLARITY images. SSD matching failed to register the the bright corpus callosum in the CLARITY brain to the dark corpus callosum of the ARA. Bright areas of the CLARITY brain were distorted resulting in the misalignment of deeper structures (Fig. 4a). Images aligned by MI-LDDMM did not have these problems (Fig. 4b).

Figure 5 shows the MI-LDDMM registration results for this CLARITY image in more detail. Qualitative examination of the CLARITY-ARA checkerboard pattern showed that most deep structures were aligned correctly (3rd row of Fig. 5). Furthermore the deformation grid's lack of singularities suggests that the computed transform ϕ_{10} was diffeomorphic (last row of Fig. 5).

Figure 6 plots the matching term $M(I(1), J_1)$ for MI-LDDMM at each iteration normalized to a range of $[0, 1]$.



(a) SSD-LDDMM



(b) MI-LDDMM

Figure 4: Comparison of SSD-LDDMM and MI-LDDMM registration for a CLARITY mouse brain. Panes (a) and (b) have an ARA coronal slice on the left juxtaposed to the corresponding aligned CLARITY slice on the right. Green arrows point out that the corpus callosum is misaligned by SSD matching but aligned correctly by MI matching. Red arrows show that SSD-LDDMM distorts bright regions but MI-LDDMM does not.

The normalized value was defined as the ratio

$$\frac{M(I(1), J_1) - M(J_1, J_1)}{M(I_0, J_1) - M(J_1, J_1)} \quad (12)$$

where a maximum value of 1 indicates the worst case scenario in which no registration occurred. A value of 0 indicates the best possible value in which the deformed template is identical to the target: $I(1) = J_1$. As expected the matching term decreased at each iteration.

3.3. Multi-scale

Two of the well-known limitations of LDDMM are on the one hand the numerical complexity and computational time of the method and on the other the non-convexity of the functional that is minimized which can lead to local minima.

In our examples, registration at a $50 \mu m$ scale can take several hours to complete on a personal computer. One way to reduce the number of iterations and thus the optimiza-

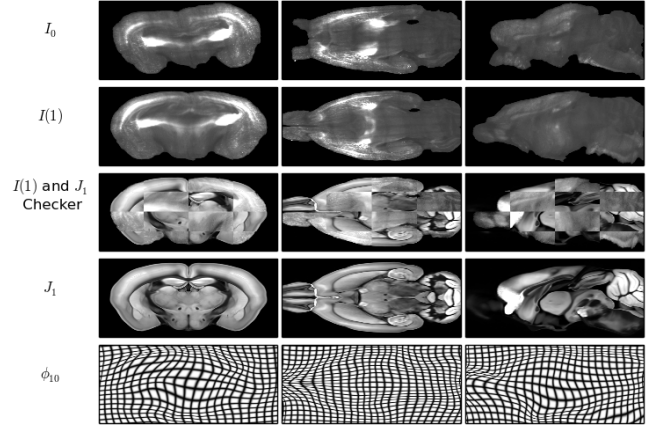


Figure 5: Detailed MI-LDDMM registration results for a CLARITY mouse brain. First, second and third columns are coronal, axial and sagittal slices respectively. First row and fourth row are CLARITY template and ARA target respectively. Second and third rows are the deformed template and its checkerboard pattern with the ARA. Final row is the deformation grid.

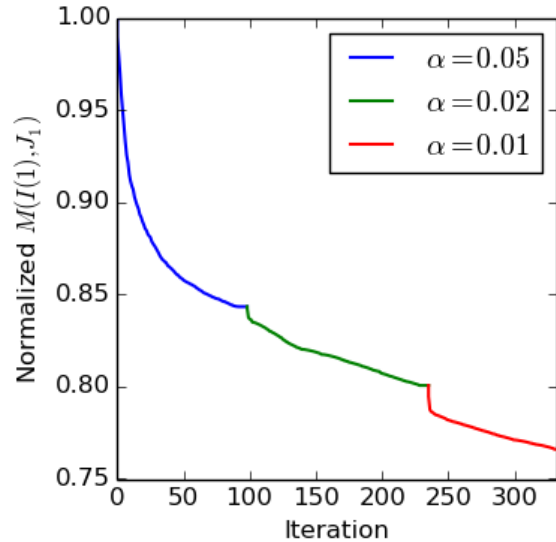


Figure 6: Matching term $M(I(1), J_1)$ at each iteration of MI-LDDMM normalized using equation (12).

tion time is to use a cascaded multi-scale approach. In the next experiment, MI-LDDMM was ran on all 11 CLARITY brains at $800 \mu m$, $400 \mu m$, $200 \mu m$, $100 \mu m$ and then $50 \mu m$ resolutions with $\alpha = 0.02$. Taking advantage of ITK's multi-resolution infrastructure [20], alignment at each level was used to initialize the alignment at the next level using trilinear interpolation from coarse to fine grid. These results were compared to a single-scale alignment at $50 \mu m$.

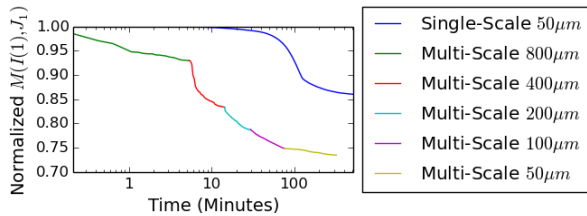


Figure 7: Matching term $M(I(1), J_1)$, normalized using equation (12), at each iteration of the single and multi-scale MI-LDDMM.

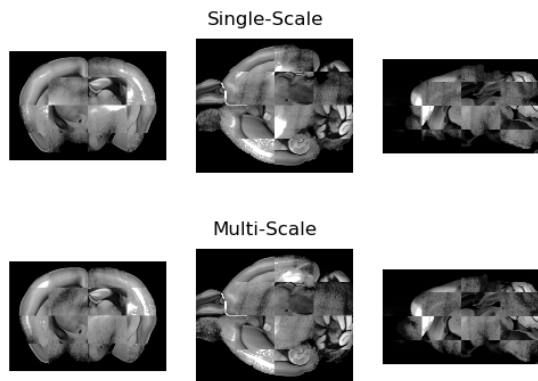


Figure 8: Checkerboard patterns of CLARITY volume $I(1)$ and the ARA average J_1 in single and multi-scale MI-LDDMM.

Figure 7 compares the timing profiles of the multi-scale and single-scale optimizations for one of the CLARITY brains. It's clear that the multi-scale optimizations ran faster than in the single-scale trial. For example, it took the normalized $M(I(1), J_1)$ over 100 minutes to decline below 0.9 in the single-scale experiment. In the multi-scale experiment this occurred in less than 10 minutes. The multi-scale registration was also more optimal as it terminated at a lower $M(I(1), J_1)$ value (Fig. 7) thus leading to a better solution by avoiding potentially suboptimal local minima. The CLARITY-ARA checkerboard pattern in Figure 8 shows that the single and multi-scale runs yielded similar results for this particular brain.

4. Conclusion

We demonstrated in this paper how the original image LDDMM framework could be generalized from SSD to MI matching by taking an optimal control point of view. An algorithm was developed and 2D experiments showed that MI-LDDMM outperformed SSD-LDDMM when the template and target differed greatly in gray level values. In 3D experiments, MI matching proved effective in aligning

CLARITY image volumes to a standard mouse atlas. A multi-scale approach was then shown to improve the rate and quality of the optimization. Future work may involve adding cross-correlation to our implementation and performing comparisons to mutual information matching. At full resolution, neural cell bodies and their axons are visible in CLARITY images. Hence we also hope to use atlas registration to map the locations and paths of these axons throughout the brain.

References

- [1] Technical white paper: Allen reference atlas - version 2. Technical report, Allen Institute for Brain Science, 2011. 3
- [2] Technical white paper: Allen mouse common coordinate framework. Technical report, Allen Institute for Brain Science, May 2015. 3
- [3] V. Arsigny, O. Commowick, X. Pennec, and N. Ayache. A log-euclidean polyaffine framework for locally rigid or affine registration. *Biomedical Image Registration: Third International Workshop Proceedings*, pages 120–127, 2006. 1
- [4] B. B. Avants, C. L. Epstein, M. Grossman, and J. C. Gee. Symmetric diffeomorphic image registration with cross-correlation: Evaluating automated labeling of elderly and neurodegenerative brain. *Medical Image Analysis*, 12(1):26–41, 2007. 2
- [5] B. B. Avants, N. J. Tustison, G. Song, P. A. Cook, A. Klein, and J. C. Gee. A reproducible evaluation of ants similarity metric performance in brain image registration. *NeuroImage*, 54(1):20332044, 2011. 2
- [6] B. B. Avants, N. J. Tustison, G. Song, B. Wu, M. Stauffer, M. M. McCormick, H. J. Johnson, J. C. Gee, and The Insight Software Consortium. A unified image registration framework for ITK. In *Biomedical Image Registration*, volume 7359, pages 266–275. Springer-Verlag, 2012. 2
- [7] M. F. Beg, M. I. Miller, A. Trounev, and L. Younes. Computing large deformation metric mappings via geodesic flows of diffeomorphisms. *International Journal of Computer Vision*, 61(2):139–157, 2005. 1, 2, 4
- [8] A. Bria and G. Iannello. TeraStitcher - A tool for fast automatic 3D-stitching of teravoxel-sized microscopy images. *BMC Bioinformatics*, 13(316), 2012. 5
- [9] R. Burns, W. G. Roncal, D. Kleissas, K. Lillaney, P. Manavalan, E. Perlman, D. R. Berger, D. D. Bock, K. Chung, L. Grosenick, N. Kasthuri, N. C. Weiler, K. Deisseroth, M. Kazhdan, J. Lichtman, R. C. Reid, S. J. Smith, A. S. Szalay, J. T. Vogelstein, and R. J. Vogelstein. The Open Connectome Project data cluster: Scalable analysis and vision for high-throughput neuroscience. *Proceedings of the 25th International Conference on Scientific and Statistical Database Management*, 2013. 5
- [10] Y. Cao, M. I. Miller, S. Mori, R. L. Winslow, and L. Younes. Diffeomorphic matching of diffusion tensor images. In *Proceedings of the IEEE Conference on Computer Vision and Pattern Recognition*, 2006. 1
- [11] C. Ceritoglu, K. Oishi, X. Li, M.-C. Chou, L. Younes, M. Albert, C. Lyketsos, P. C. van Zijl, M. I. Miller, and S. Mori.

- Multi-contrast large deformation diffeomorphic metric mapping for diffusion tensor imaging. *NeuroImage*, 47(2):618–627, 2009. 1
- [12] N. Charon and A. Trouvé. The varifold representation of nonoriented shapes for diffeomorphic registration. *SIAM Journal on Imaging Sciences*, 6(4):2547–2580, 2013. 1
- [13] K. Chung, J. Wallace, S.-Y. Kim, S. Kalyanasundaram, A. S. Andalman, T. J. Davidson, J. J. Mirzabekov, K. A. Zalusky, J. Mattis, A. K. Denisin, S. Pak, H. Bernstein, L. G. Charu Ramakrishnan, V. Gradinaru, and K. Deisseroth. Structural and molecular interrogation of intact biological systems. *Nature*, 497:332–337, 2013. 2
- [14] T. M. Cover and J. A. Thomas. *Elements of Information Theory*. John Wiley & Sons, Inc., 2 edition, 2006. 2
- [15] B. Dogdas, D. Stout, A. F. Chatzioannou, and R. M. Leahy. Digimouse: a 3D whole body mouse atlas from CT and cryosection data. *Physics in Medicine and Biology*, 52(3):577–587, 2007. 2
- [16] E. S. Lein *et al.* Genome-wide atlas of gene expression in the adult mouse brain. *Nature*, 445:168–176, 2007. 2
- [17] J. Glaunès, A. Trouvé, and L. Younes. Diffeomorphic matching of distributions: a new approach for unlabelled point-sets and sub-manifolds matching. In *Proceedings of the IEEE Conference on Computer Vision and Pattern Recognition*, volume 2, 2004. 1
- [18] G. L. Hart, C. Zach, and M. Niethammer. An optimal control approach for deformable registration. In *IEEE Computer Society Conference on Computer Vision and Pattern Recognition Workshop*, 2009. 3
- [19] G. A. Johnson, A. Badea, J. Brandenburg, G. Cofer, B. Fubara, S. Liu, and J. Nissarov. Waxholm space: An image-based reference for coordinating mouse brain research. *NeuroImage*, 53(1):365–372, 2010. 2
- [20] H. J. Johnson, M. M. McCormick, and L. Ibáñez. *The ITK Software Guide Book 2: Design and Functionality*. The Insight Software Consortium, 4 edition, July 2016. 2, 4, 6
- [21] A. R. Jones, C. C. Overly, and S. M. Sunkin. The Allen Brain Atlas: 5 years and beyond. *Nature Reviews Neuroscience*, 10:821–828, 2009. 3
- [22] S. C. Joshi and M. I. Miller. Landmark matching via large deformation diffeomorphisms. *IEEE Transactions on Image Processing*, 9(8):1357–2000, 2000. 1
- [23] S.-Y. Kim, K. Chung, and K. Deisseroth. Light microscopy mapping of connections in the intact brain. *Trends in Cognitive Sciences*, 17(12):596–599, 2013. 2
- [24] K. S. Kuttan, J. T. Vogelstein, N. Charon, L. Ye, K. Deisseroth, and M. I. Miller. Deformably registering and annotating whole CLARITY brains to an atlas via masked LD-DMM. In *Proc SPIE 9896: Optics, Photonics and Digital Technologies for Imaging Applications IV*, 2016. 3
- [25] D. Mattes, D. R. Haynor, H. Vesselle, T. K. Lewellen, and W. Eubank. Nonrigid multimodality image registration. In M. Sonka and K. M. Hanson, editors, *Proc. SPIE 4322, Medical Imaging: Image Processing*, pages 1609–1620, 2001. 4
- [26] M. I. Miller, A. Trouvé, and L. Younes. Hamiltonian systems and optimal control in computational anatomy: 100 years since D’Arcy Thompson. *Annual Review of Biomedical Engineering*, 17:447–509, 2015. 3
- [27] J. P. W. Pluim, A. Maintz, and M. A. Viergever. Mutual-information-based registration of medical images: a survey. *IEEE Transactions on Medical Imaging*, 22(8):986–1004, 2003. 2
- [28] S. Reaungamornrat, T. De Silva, A. Uneri, S. Vogt, G. Kleinszig, A. J. Khanna, J.-P. Wolinsky, J. L. Prince, and J. H. Siewerdsen. MIND demons: Symmetric diffeomorphic deformable registration of MR and CT for image-guided spine surgery. *IEEE Transactions on Medical Imaging*, 35(11):2413–2424, 2016. 2
- [29] S. Reaungamornrat, T. De Silva, A. Uneri, J.-P. Wolinsky, A. J. Khanna, G. Kleinszig, S. Vogt, J. L. Prince, and J. H. Siewerdsen. MIND demons for MR-to-CT deformable image registration in image-guided spine surgery. In *Proc. SPIE Medical Imaging 2016: Image-Guided Procedures, Robotic Interventions, and Modeling*, volume 9798, 2016. 2
- [30] D. Rueckert, L. I. Sonoda, C. Hayes, D. L. G. Hill, M. O. Leach, and D. J. Hawkes. Nonrigid registration using free-form deformations: application to breast MR images. *IEEE Transactions on Medical Imaging*, 18(8):712–721, 1999. 1
- [31] A. Staniforth and J. Côté. Semi-lagrangian integration schemes for atmospheric models: a review. *Monthly Weather Review*, 119:2206–2223, 1991. 4
- [32] R. Tomer, L. Ye, B. Hsueh, and K. Deisseroth. Advanced CLARITY for rapid and high-resolution imaging of intact tissues. *Nature Protocols*, 9(7):1682–1697, 2014. 2, 5
- [33] M. Vaillant and J. Glaunès. Surface matching via currents. In G. E. Christensen and M. Sonka, editors, *Information Processing in Medical Imaging*, pages 381–392, 2005. 1
- [34] T. Vercauteren, X. Pennec, A. Perchant, and N. Ayache. Diffeomorphic demons: Efficient non-parametric image registration. *NeuroImage*, 45(1):61–72, 2009. Mathematics in Brain Imaging. 1
- [35] F.-X. Vialard, L. Risser, D. Rueckert, and C. J. Cotter. Diffeomorphic 3D image registration via geodesic shooting using an efficient adjoint calculation. *International Journal of Computer Vision*, 97(2):229–241, 2012. 2
- [36] P. Viola and W. M. Wells. Alignment by maximization of mutual information. *International Journal of Computer Vision*, 24(2):137–154, 1997. 2